



HAL
open science

Earth rotation prevents exact solid-body rotation of fluids in the laboratory

Jean Boisson, D Cébron, Frederic Moisy, Pierre-Philippe Cortet

► **To cite this version:**

Jean Boisson, D Cébron, Frederic Moisy, Pierre-Philippe Cortet. Earth rotation prevents exact solid-body rotation of fluids in the laboratory. EPL - Europhysics Letters, 2012, pp.59002. 10.1209/0295-5075/98/59002 . hal-01152731

HAL Id: hal-01152731

<https://hal.science/hal-01152731>

Submitted on 18 May 2015

HAL is a multi-disciplinary open access archive for the deposit and dissemination of scientific research documents, whether they are published or not. The documents may come from teaching and research institutions in France or abroad, or from public or private research centers.

L'archive ouverte pluridisciplinaire **HAL**, est destinée au dépôt et à la diffusion de documents scientifiques de niveau recherche, publiés ou non, émanant des établissements d'enseignement et de recherche français ou étrangers, des laboratoires publics ou privés.

Earth rotation prevents exact solid-body rotation of fluids in the laboratory

J. BOISSON^{1(a)}, D. CÉBRON^{2(b)}, F. MOISY^{1(c)} and P.-P. CORTET^{1(d)}

¹ *Laboratoire FAST, CNRS, Univ Paris-Sud, UPMC Univ Paris 06 - France, EU*

² *Institut für Geophysik, ETH Zürich - Switzerland*

received 1 April 2012; accepted in final form 18 May 2012
published online 12 June 2012

PACS 92.10.Ei – Coriolis effects
PACS 47.32.-y – Vortex dynamics; rotating fluids
PACS 92.10.hj – Internal and inertial waves

Abstract – We report direct evidence of a secondary flow excited by the Earth rotation in a water-filled spherical container spinning at constant rotation rate. This so-called *tilt-over flow* essentially consists in a rotation around an axis which is slightly tilted with respect to the rotation axis of the sphere. In the astrophysical context, it corresponds to the flow in the liquid cores of planets forced by precession of the planet rotation axis, and it has been proposed to contribute to the generation of planetary magnetic fields. We detect this weak secondary flow using a particle image velocimetry system mounted in the rotating frame. This secondary flow consists in a weak rotation, thousand times smaller than the sphere rotation, around a horizontal axis which is stationary in the laboratory frame. Its amplitude and orientation are in quantitative agreement with the theory of the tilt-over flow excited by precession. These results show that setting a fluid in a perfect solid-body rotation in a laboratory experiment is impossible —unless by tilting the rotation axis of the experiment parallel to the Earth rotation axis.

Copyright © EPLA, 2012

Introduction. – There are few examples of fluid mechanics experiments at the laboratory scale in which the Earth’s Coriolis force has a measurable influence. Such experiments may be considered as fluid analogues to the Foucault pendulum. The most popular instance is certainly the drain of a bathtub vortex [1]. Although this is the subject of common misconception, it is actually possible to detect the influence of the Earth’s rotation on the vortex, but only under extremely careful experimental conditions, far from the everyday experience [2]. Thermal convection is another example, in which a slow drift of the large-scale flow due to the Earth rotation has been detected in very controlled systems [3,4].

In this letter we describe an experiment which may be considered as the most simple fluid Foucault pendulum: it consists in a volume of water enclosed in a spherical container spinning at constant rotation rate Ω_0 (fig. 1). After a transient known as spin-up, the water is expected to rotate as a solid body at the same rate Ω_0 [5]. The timescale for this spin-up is classically given by the

Ekman time $\tau_E = R(\nu\Omega_0)^{-1/2}$, where R is the radius of the sphere and ν the kinematic viscosity of the fluid. For a typical laboratory experiment using water, this timescale is usually of the order of a minute, so after a few tens of minutes a perfect solid-body rotation should be reached, with the fluid exactly at rest in the frame of the container. If this simple experiment is performed on Earth, it is expected that the Earth rotation could prevent from reaching this idealized solid rotation state [6,7]. A weak secondary flow, known as *tilt-over* flow [5,8,9], is induced by the precession of the rotation vector $\mathbf{\Omega}_0$ of the container by the Earth rotation vector $\mathbf{\Omega}_p$. Seen from the laboratory frame of reference, the fluid particles rotating at velocity $\mathbf{u}_0 = \mathbf{\Omega}_0 \times \mathbf{r}$ experience a Coriolis force per unit mass $\mathbf{f}_c = -2\mathbf{\Omega}_p \times \mathbf{u}_0$. This Coriolis force disturbs the fluid particles periodically at frequency Ω_0 , and tends to deflect their trajectory towards the plane normal to $\mathbf{\Omega}_p$.

Precession driven flows in spherical or spheroidal containers and in spheroidal shells have received considerable interest since Poincaré [10], because of their importance to geophysical and astrophysical flows [8,9]. In the case of the Earth, rotating with a period $T_0 \sim 1$ day, the precession of its rotation axis, at a period $T_p \simeq 26000$ years, could produce large excursions of the

^(a)E-mail: boisson@fast.u-psud.fr

^(b)E-mail: david.cebtron@erdw.ethz.ch

^(c)E-mail: moisy@fast.u-psud.fr

^(d)E-mail: ppcortet@fast.u-psud.fr

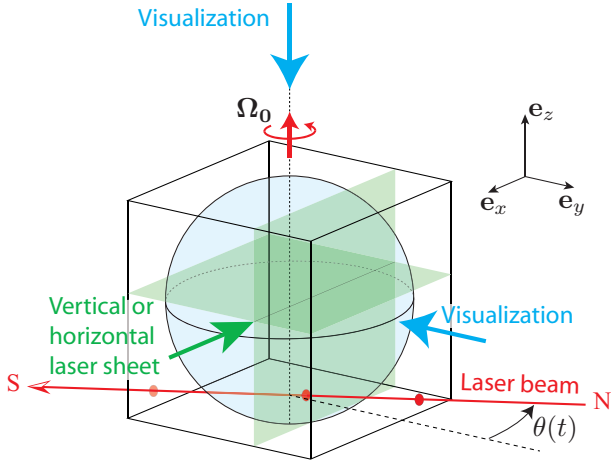


Fig. 2: (Color online) Schematic view of the cubic water tank containing the 115 mm radius glass sphere, mounted together on the rotating platform. PIV measurements are achieved in off-centered vertical and horizontal planes, located at $y_{\text{mes}} = +22$ mm and $z_{\text{mes}} = +22$ mm, using a corotating laser sheet and a camera aiming normally at it. The angle $\theta(t)$ between the images and the North direction is determined using a continuous laser beam aligned along the North-South orientation and crossing the rotation axis.

a Poincaré number Ω_p/Ω_0 ranging from 3.5×10^{-4} to 4.3×10^{-5} .

After the start of the platform rotation, we wait at least $\tau_w = 2$ hours before data acquisition in order to reach a stationary regime. This waiting time represents at least $30 \tau_E$, where $\tau_E = R(\nu\Omega_0)^{-1/2}$ is the Ekman spin-up time. This indicates that the solid-body rotation state should be reached, apart from precession effects, with a relative precision better than $\exp(-\tau_w/\tau_E) \simeq 10^{-13}$.

Velocity fields are measured in the rotating frame using a two-dimensional PIV system [15] mounted on the rotating platform, in either a vertical ($\mathbf{e}_x, \mathbf{e}_z$)- or a horizontal ($\mathbf{e}_x, \mathbf{e}_y$)-plane (fig. 2). These measurement planes are off-centered, at $y_{\text{mes}}/R = z_{\text{mes}}/R \simeq 0.19$ (see fig. 2), in order to get better insight in the spatial structure of the flow. Optical distortions are reduced by immersing the glass sphere in a square glass tank of 300 mm side also filled with water. The distortion is found less than 5% for $r < 0.9R$. The fluid is seeded with $10 \mu\text{m}$ tracer particles, and illuminated by a corotating laser sheet generated by a 140 mJ Nd:YAG pulsed laser. For both horizontal and vertical measurements, the sphere cross-section is imaged with a high-resolution 2048×2048 pixels camera aiming normally at the laser sheet.

For each rotation rate Ω_0 , a set of 2000 images is acquired, covering at least 80 rotation periods. The sampling rate is synchronized with the platform rotation rate, with a number of images per rotation ranging from 24 (for low Ω_0) to 9 (for large Ω_0). PIV fields are computed over successive images using 32×32 pixels interrogation windows with 50% overlap, leading to a spatial resolution of about 2 mm. This resolution is not enough to resolve the thickness of the Ekman boundary

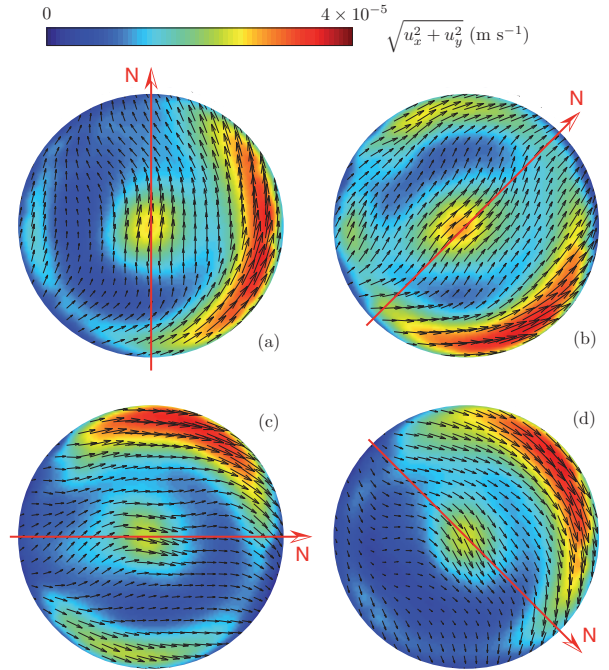


Fig. 3: (Color online) Horizontal velocity fields measured in the rotating frame, in the off-centered horizontal plane at $z_{\text{mes}}/R \simeq 0.19$ for $\Omega_0 = 6$ rpm ($E = 1.2 \times 10^{-4}$), with a phase shift of $\pi/4$ between each image. The platform rotation is anticlockwise. The red arrows indicate the direction of the North at each time. Resolution of the velocity fields has been reduced by a factor 5 for better visibility.

layers, $\delta \simeq R E^{1/2} = 0.8\text{--}2.2$ mm, but is appropriate for the large scales of the precession flow expected in the bulk.

In view of the very low velocity expected for the precession flow, the resolution of the velocity measurement is critical in our experiment. The characteristic velocities of the flow encountered in this work ranges from 0.01 to 0.4 mm s^{-1} for Ω_0 between 2 and 16 rpm. For the sampling rates considered here, these velocities correspond to a typical frame-by-frame particle displacement of 0.16 to 2.6 pixels only. Although very weak, such displacement may actually be measured using PIV with sub-pixel interpolation of the correlation peak. For interrogation windows of size 32×32 pixels, an accuracy of 0.05 pixel can be achieved using this technique [15,16], yielding a signal-to-noise ratio ranging from 3 (low Ω_0) to 50 (large Ω_0).

The orientation of the experiment with respect to the Earth rotation axis is monitored using a continuous laser beam aligned along the North-South direction and passing through the rotation axis of the sphere (see fig. 2). The beam crosses the cubic glass tank and is therefore visible on the recorded images. The angle $\theta(t)$ between the South-North direction and the measurement fields (see fig. 2) can be determined for each image with a precision better than $\pm 0.5^\circ$.

Structure of the tilt-over flow. – We first show in fig. 3 the flow measured in the horizontal plane in the rotating frame for a rotation rate $\Omega_0 = 6$ rpm. This flow

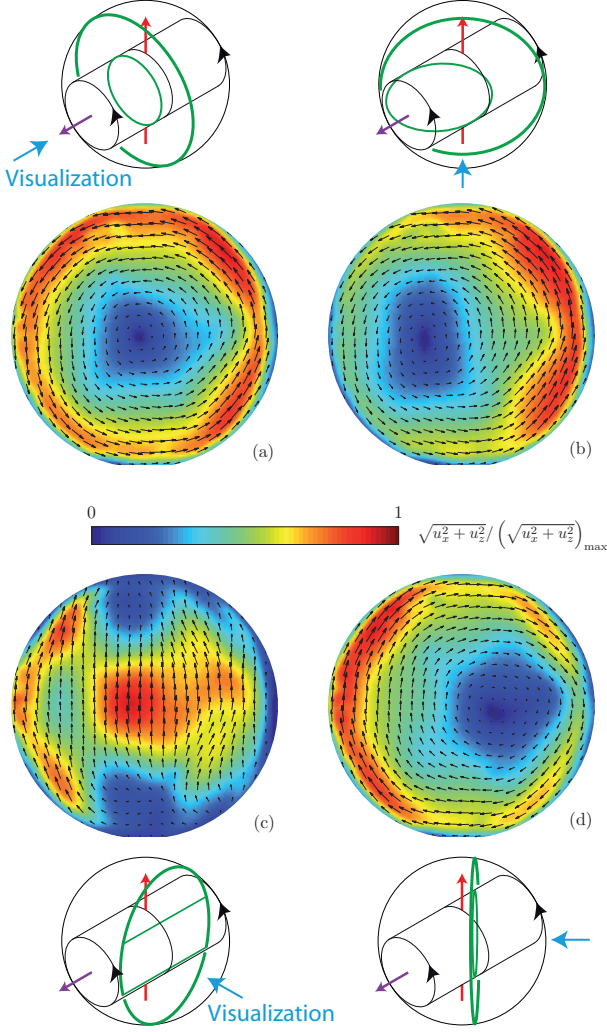


Fig. 4: (Color online) Vertical velocity fields measured in the rotating frame, in the off-centered vertical plane at $y_{\text{mes}}/R \simeq 0.19$ for $\Omega_0 = 6$ rpm ($E = 1.2 \times 10^{-4}$), with a phase shift of $\pi/4$ between each image. The color maps the vertical velocity norm normalized by its maximum in each field. The phase origin is not the same as in fig. 3.

represents the departure between the total flow in the laboratory frame and the solid-body rotation at Ω_0 . In order to improve the quality of the velocity fields shown here, a phase average is performed over the velocity fields at the platform rotation rate Ω_0 . This procedure allows to decrease the broad-band PIV measurement noise by a factor $N^{1/2}$, where N is the number of recorded rotation periods ($N \geq 80$). The spatial structure of the precession flow can finally be extracted with a signal-to-noise ratio of at least 30 for all rotations rates.

The four snapshots shown in fig. 3 are separated by a phase shift of $\pi/4$, with a phase origin chosen such that $\mathbf{e}_x = \mathbf{e}_1$ (*i.e.*, \mathbf{e}_y pointing to the North). In spite of the very weak velocity signal (of order of 0.04 mm s^{-1} , to be compared to the typical velocity of the sphere boundaries, $\Omega_0 R \simeq 72 \text{ mm s}^{-1}$), we clearly observe a well-defined flow pattern, which is rotating as a whole at the platform

rotation rate but in the opposite direction. This weak flow is therefore stationary in the laboratory frame. Assuming that the total flow in the laboratory frame is a solid-body rotation of vector $\boldsymbol{\omega}$ slightly tilted with respect to $\boldsymbol{\Omega}_0$, the measured flow must be a solid-body rotation of rotation vector $\boldsymbol{\omega}' = \boldsymbol{\omega} - \boldsymbol{\Omega}_0$. Since the measurement plane is shifted at $z_{\text{mes}}/R \simeq 0.19$, the resulting horizontal velocity field must be uniform in the bulk, given by $\boldsymbol{\omega}' \times (z_{\text{mes}} \mathbf{e}_3)$, and rotating in the anticyclonic direction at frequency Ω_0 , which is precisely what we observe. Snapshots at other values of Ω_0 show essentially the same flow patterns.

Measurements in the vertical plane, shown in fig. 4, confirm this flow structure. In this configuration, the camera is now rotating around the vortex of quasi-horizontal rotation vector $\boldsymbol{\omega}'$ stationary in the laboratory frame. The 4 snapshots taken over half a rotation around the vortex actually show the following sequence: (a) anticlockwise, with $\boldsymbol{\omega}'$ pointing towards the camera; (b) intermediate; (c) ascending, with $\boldsymbol{\omega}'$ pointing to the left; (d) intermediate. If the tilt-over flow were a pure solid-body rotation, the ascending flow in the snapshot (c) would be uniform, given by $\boldsymbol{\omega}' \times (y_{\text{mes}} \mathbf{e}_y)$, which is approximately the case far from the boundaries. The wall region where the flow departs from a pure uniform flow has a thickness of order of $0.3 R$, which is much larger than the expected Ekman thickness $E^{1/2} R \simeq 0.01 R$. The tilt-over flow is therefore not exactly a pure solid-body rotation, in agreement with numerical results obtained in a spherical shell with a very small stress-free inner solid core [17]. Indeed, because of the breakdown of the Ekman layer at the so-called critical circles, a pure solid-body rotation cannot be a uniformly valid solution [14].

Viscous prediction for the tilt-over flow forced by precession.

– We compute here the rotation vector $\boldsymbol{\omega}$ in the bulk of the fluid viewed from the precessing frame of reference (here the laboratory frame), following refs. [18,19]. The differential rotation between the fluid in the bulk rotating at $\boldsymbol{\omega}$ and the sphere boundary rotating at $\boldsymbol{\Omega}_0$ is matched across an Ekman boundary layer of typical thickness $RE^{1/2}$. We therefore assume $E \ll 1$, such that a separation between a bulk flow and a thin boundary layer may be assumed. In the steady state, the viscous torque $\boldsymbol{\Gamma}_\nu$ exerted by the boundary layers on the fluid in the bulk is balanced by the Coriolis torque $\boldsymbol{\Gamma}_c$ (note that the pressure torque is zero here because of spherical symmetry). This balance, projected along $\boldsymbol{\omega}$ and along two directions normal to $\boldsymbol{\omega}$, yields the following nonlinear system of equations [5,19],

$$\omega_1^2 + \omega_2^2 = \omega_3(\Omega_0 - \omega_3), \quad (2)$$

$$\frac{\Omega_p}{\sqrt{E}} (\omega_3 \cos \Lambda - \omega_2 \sin \Lambda) = \lambda_r \omega_1 \omega_3^{1/4} \Omega_0^{3/4} + \lambda_i \omega_2 \frac{\Omega_0^{5/4}}{\omega_3^{1/4}}, \quad (3)$$

$$\frac{\Omega_p}{\sqrt{E}} \omega_1 \cos \Lambda = \lambda_r \Omega_0^{3/4} \omega_3^{1/4} (\Omega_0 - \omega_3), \quad (4)$$

where λ_r and λ_i are, respectively, the non-dimensional viscous damping rate and viscous correction to the eigenfrequency of the tilt-over mode. Their values have been obtained by Greenspan [5] and completed by Zhang *et al.* [20], $\lambda_r = -2.62$ and $\lambda_i = 0.258$. In presence of viscosity, the eigenfrequency Ω_0 of the inviscid tilt-over mode becomes $\Omega_0 + (\lambda_i + i\lambda_r)\sqrt{E}\sqrt{\Omega_0\omega}$ [18,20], which means that, if the precession forcing is switched off, the tilt-over mode starts to rotate in the inertial frame at a frequency $\lambda_i\sqrt{E}\sqrt{\Omega_0\omega}$, while exponentially decaying at a rate $|\lambda_r|\sqrt{E}\sqrt{\Omega_0\omega}$.

Equation (2) reflects the fact that the work done per unit time by the viscous torque is zero, $\mathbf{\Gamma}_\nu \cdot \boldsymbol{\omega} = 0$, since the work done by the Coriolis force is zero by definition. This equation, which can be recast into $\boldsymbol{\omega} \cdot (\boldsymbol{\omega} - \boldsymbol{\Omega}_0) = 0$, simply expresses the so-called “no spin-up” condition, indicating that there is no differential rotation between the fluid and the sphere in the direction of the fluid rotation. This right angle between $\boldsymbol{\omega}$ and $\boldsymbol{\omega}' = \boldsymbol{\omega} - \boldsymbol{\Omega}_0$ indicates that the rotation rate $|\boldsymbol{\omega}|$ of the fluid is lower than Ω_0 .

If we further assume that the Poincaré number Ω_p/Ω_0 is small compared to $E^{1/2}$, the rotation vector $\boldsymbol{\omega}$ is almost aligned with $\boldsymbol{\Omega}_0$, and the system of equations (2)–(4) can be simplified. More precisely, this regime applies for rotation rates $\Omega_0 \gg \Omega_{0,c}$, with

$$\Omega_{0,c} = \left(\frac{\Omega_p R \sin \Lambda}{\lambda_r \sqrt{\nu}} \right)^2. \quad (5)$$

This condition is comfortably satisfied in the present experiments, with $\Omega_{0,c} \simeq 5.2 \times 10^{-5}$ rpm. In this limit, the components of the tilt-over flow can be explicitly derived

$$\omega_1 \simeq \frac{\Omega_p \cos \Lambda}{\lambda_r} \left(\frac{\Omega_0 R^2}{\nu} \right)^{1/2}, \quad (6)$$

$$\omega_2 \simeq \frac{\lambda_i}{\lambda_r} \omega_1, \quad (7)$$

$$\omega_3 \simeq \Omega_0. \quad (8)$$

The horizontal projection of $\boldsymbol{\omega}$ in the laboratory frame, $\boldsymbol{\omega}_h = \omega_1 \mathbf{e}_1 + \omega_2 \mathbf{e}_2$, has therefore an amplitude

$$\omega_h = \frac{\Omega_p \cos \Lambda}{|\lambda_r|} \left(\frac{\Omega_0 R^2}{\nu} \right)^{1/2} \left(1 + \frac{\lambda_i^2}{\lambda_r^2} \right)^{1/2}, \quad (9)$$

which has indeed the expected form (1). Note that, in the limit considered here ($\Omega_p/\Omega_0 \ll \sqrt{E}$), the horizontal projection $\boldsymbol{\omega}_h$ measured in the experiment almost coincides with $\boldsymbol{\omega}'$.

In this limit, the angle φ between $\boldsymbol{\omega}_h$ and \mathbf{e}_1 (the East direction) is constant, and given by

$$\varphi = \arctan \left(\frac{\omega_2}{\omega_1} \right) = \arctan \frac{\lambda_i}{\lambda_r} = 174.35^\circ, \quad (10)$$

showing that $\boldsymbol{\omega}_h$ points almost to the West (along $-\mathbf{e}_1$), with a slight component to the North. Remarkably, this

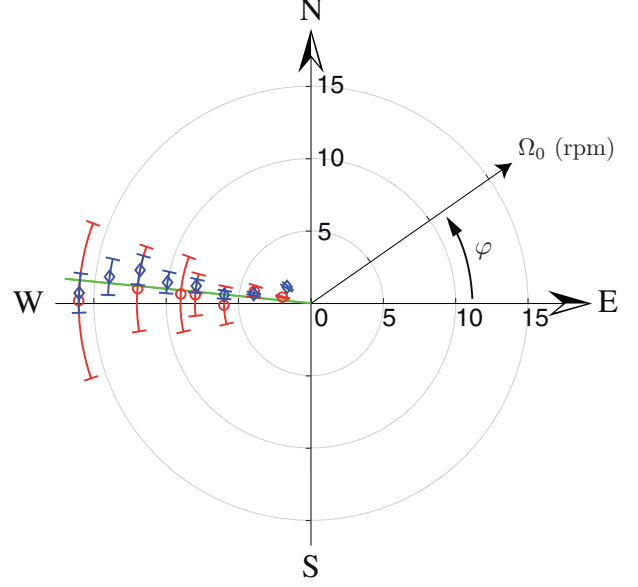


Fig. 5: (Color online) Angle φ between the rotation vector of the tilt-over flow and \mathbf{e}_1 (*i.e.*, East) as a function of the rotation rate Ω_0 in polar coordinates. Measurements are obtained in the horizontal (\circ) and the vertical (\diamond) plane, respectively. The continuous line shows the theoretical prediction $\varphi = 174.35^\circ$ (10).

asymptotic angle obtained in the limit of large Ω_0 is almost perpendicular to the inviscid prediction of Poincaré, for which $\boldsymbol{\omega}_h$ points to the North (*i.e.*, $\varphi = 90^\circ$). This indicates that, even for very low viscosity, the boundary layers have a critical influence on the tilt-over flow, provided that $\Omega_p/\Omega_0 \ll E^{1/2}$.

Comparison with the experimental tilt-over flow.

– The rotation rate ω_h of the tilt-over flow and its angle φ with the East have been systematically determined for Ω_0 ranging from 2 to 16 rpm. These data have been extracted independently from the raw velocity fields measured in the vertical and horizontal planes, and are compared here with the theoretical predictions (9) and (10) in figs. 5 and 6.

Measurements of the vortex angle φ from the PIV data in the vertical plane have been obtained as follows: the horizontal vorticity, spatially averaged over a central region of 50 mm radius, shows a harmonic oscillation at frequency Ω_0 . At each period, the delay between the time t_{\max} of maximum vorticity (when $\boldsymbol{\omega}_h$ points to the camera) and the time at which the North-South laser beam is aligned with the camera axis is computed. Knowing the instantaneous angle $\theta(t)$ between the camera incidence and the South-North direction, we can simply deduce the angle of the vortex as $\varphi = \theta(t_{\max}) + 90^\circ$. An independent estimate for φ has been determined from the data in the horizontal plane, by computing the time-averaged (and spatially averaged over the region $|\mathbf{r}| < 50$ mm) angle of the velocity with respect to the East direction \mathbf{e}_1 .

The rotation rate ω_h of the horizontal component of the tilt-over flow has been determined from the vertical cuts

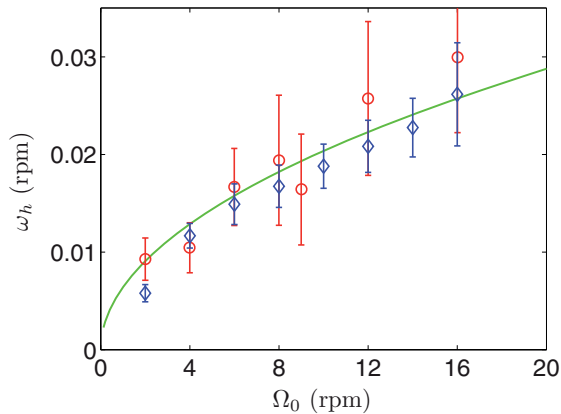


Fig. 6: (Color online) Horizontal rotation rate ω_h of the tilt-over flow as a function of the rotation rate of the platform Ω_0 , measured in the horizontal (\circ) and vertical (\diamond) planes. The continuous line shows the prediction (9).

as half the spatially averaged (over a central disk of radius 50 mm) vorticity, measured at the times t_{\max} of maximum vorticity. ω_h has also been determined independently from the horizontal cuts, as $\omega_h = \langle |\mathbf{u}_h| \rangle / z_{\text{mes}}$, where $\langle \cdot \rangle$ is an average over time and over the region $|\mathbf{r}| < 50$ mm, and z_{mes} is the height of the measurement plane.

For both measurements in the horizontal and vertical planes, one value of φ and ω_h is obtained at each rotation period. From this set, the average and standard deviation are computed over the 80 periods recorded for each rotation rate. In addition to the temporal fluctuations, the errorbars in figs. 5 and 6 also include the variations of φ and ω_h when varying the radius of the averaging region between 25 and 75 mm. For both quantities, the estimates determined from the two measurement planes closely agree, although data from the horizontal plane systematically show a larger scatter.

The vortex angle measured from both vertical and horizontal planes, $\varphi \simeq 173 \pm 4^\circ$ and $175 \pm 11^\circ$, respectively (fig. 5), are in good agreement with the theoretical prediction (10) (see footnote ¹). Similarly, the rotation rate ω_h measured in both planes closely follow the prediction (9) to within 20% over the range $\Omega_0 = 2\text{--}16$ rpm (fig. 6). The agreement of ω_h and φ with the theoretical predictions is remarkable in view of the very weak velocity signal, providing strong evidence that the weak secondary flow that we observe originates from the precession of the experiment by the Earth rotation. The magnitude of the secondary rotation lies in the range $(1.5\text{--}3) \times 10^{-3} \Omega_0$, confirming that the rotation vector $\boldsymbol{\omega}$ of the fluid is almost aligned with $\boldsymbol{\Omega}_0$, with a very weak angular departure of $\omega_h / \Omega_0 < 0.2^\circ$.

¹A possible residual ellipticity of the sphere would lead to slightly different angles φ . Considering a prolate or an oblate spheroid, of ellipticity given by the maximum deviation of the radius of the sphere ($R = 115 \pm 0.25$ mm), yields predictions for φ between 170 and 180° for the range of Ω_0 considered here, which is compatible with the present data.

Conclusion. – Measuring the influence of the Earth rotation at the laboratory scale is a technical challenge. In the fluid analogue of the Foucault pendulum presented in this letter, the very weak precession driven flow would have been impossible to detect directly from the laboratory frame. Probing the flow in the rotating frame naturally subtracts the first-order rotation and allows us to detect this slight correction. We note that such residual tilt-over flow forced by the Earth rotation defines an irreducible background flow which should be present in every rotating fluid experiments, routinely used as models for geophysical and astrophysical flows in the laboratory.

We acknowledge D. LATHROP, C. LAMRIBEN and M. RABAU for fruitful discussions, and A. AUBERTIN, L. AUFRAY, C. BORGET, A. CAMPAGNE and R. PIDOUX for experimental help. JB is supported by the “Triangle de la Physique”. This work is supported by the ANR through grant No. ANR-2011-BS04-006-01 “ONLITUR”. The rotating platform “Gyroflow” was funded by the “Triangle de la Physique”.

REFERENCES

- [1] PERROT M., *C. R. Acad. Sci.*, **XLIX** (1859) 637.
- [2] SHAPIRO A. H., *Nature*, **196** (1962) 1080.
- [3] PANTALONI J., CERISIER P., BAILLEUX R. and GERBAUD C., *J. Physique Lett.*, **42** (1981) L147.
- [4] BROWN E. and AHLERS G., *Phys. Fluids*, **18** (2006) 125108.
- [5] GREENSPAN H., *The Theory of Rotating Fluids* (Cambridge University Press, London) 1968.
- [6] VANYO J. P. and DUNN J. R., *Geophys. J. Int.*, **142** (2000) 409.
- [7] TRIANA S. A., ZIMMERMAN D. S. and LATHROP D. P., *J. Geophys. Res.*, **117** (2012) B04103.
- [8] BUSSE F. H., *J. Fluid Mech.*, **33** (1968) 739.
- [9] MALKUS W. V. R., *Science*, **160** (1968) 259.
- [10] POINCARÉ R., *Bull. Astron.*, **27** (1910) 321.
- [11] GREFF-LEFFTZ M. and LEGROS H., *Science*, **286** (1999) 1707.
- [12] KERSWELL R. R., *J. Fluid Mech.*, **321** (1996) 335.
- [13] TILGNER A., *Phys. Fluids*, **17** (2005) 034104.
- [14] KIDA S., *J. Fluid Mech.*, **680** (2011) 150.
- [15] DaVis by LaVision GmbH complemented by the PIVMat toolbox for Matlab, <http://www.fast.u-psud.fr/pivmat>.
- [16] RAFFEL M., WILLERT C., WERELEY S. and KOMPENHANS J., *Particle Image Velocimetry* (Springer-Verlag, Berlin) 2007.
- [17] TILGNER A. and BUSSE F. H., *J. Fluid Mech.*, **426** (2001) 387.
- [18] NOIR J., CARDIN P., JAULT D. and MASSON J.-P., *Geophys. J. Int.*, **154** (2003) 407.
- [19] CÉBRON D., LE BARS M. and MEUNIER P., *Phys. Fluids*, **22** (2010) 101063.
- [20] ZHANG K., LIAO X. and EARNSHAW P., *J. Fluid Mech.*, **504** (2004) 1.